Current Opinion in Solid State & Materials Science xxx (xxxx) xxx–xxx

Contents lists available at ScienceDirect

Current Opinion in Solid State & Materials Science

journal homepage: www.elsevier.com/locate/cossms

Reconfigurable nanoscale soft materials

Zihao Ou[a], Ahyoung Kim[a], Wen Huang[b], Paul V. Braun[a,c,d], Xiuling Li[b,c], Qian Chen[a,c,d,*]

[a] Department of Materials Science and Engineering, University of Illinois, Urbana, IL 61801, United States
[b] Department of Electrical and Computer Engineering, Micro and Nanotechnology Laboratory, University of Illinois, Urbana, IL 61801, United States
[c] Materials Research Laboratory, University of Illinois, Urbana, IL 61801, United States
[d] Department of Chemistry, Beckman Institute for Advanced Science and Technology, University of Illinois, Urbana, IL 61801, United States

A B S T R A C T

We discuss recent research efforts towards understanding and implementing the physical rules needed to make materials—especially materials composed of nanoscale building blocks—that exhibit the defining characteristics of living systems: adaptive and evolving functional behavior. In particular, we highlight advancements in direct imaging and quantifying of kinetic pathways governing structural reconfiguration in model systems of colloidal nanoparticles as well as emerging opportunities brought by frontier efforts in synthesizing shape-shifting colloids and flexible electronics. Direct observation of kinetic "crossroads" in nanoparticle self-assembly and reconfiguration will offer insight into how these steps can be manipulated to design dynamic, potentially novel materials and devices. Moreover, these principles will not be limited to nanoparticles; when extended to building blocks like soft micelles and proteins, they have the potential to have a similar impact throughout the broader field of soft matter physics.

1. Introduction

An emerging theme in materials science is to design and engineer materials that reconfigure, changing their structure, appearance, strength, and other properties on demand. Unlike the dominating static materials, the reconfigurable ones can respond productively to variable tasks and conditions. Macroscopic examples already in the literature include materials which enable systems ranging from shape-shifting robots that grasp and release cargos upon for example a temperature stimulus, "skins" that optimize the aerodynamics of automobiles and aircraft in response to their environment, to camouflage coatings with adaptive optical properties that match with their surroundings to avoid detection [1–4]. On the small scale, reconfigurable materials composed of nano-sized building blocks, such as nanoparticles (NPs), are also gaining increasing attention, due to their quantum confinement effect, structure-dependent coupling in properties [5,6], and potential usage as miniaturized devices [7–9], where the fundamental reconfigurable units are as small as a few nanometers. For example, great efforts have been devoted into active plasmonics with environmentally sensitive plasmonic coupling between metal NPs and optical properties [10]. The building blocks of these structures also share the same length and energy scale (as small as several $k_B T$) as building blocks in living life – biomolecules like proteins and nucleic acids. We can thus utilize such conceptual analogies between reconfiguration pathways of synthetic NP ensembles and how biomolecules sample over all the possible folding states (often categorize as healthy or diseased) on the potential energy surface that fluctuates driven by microenvironmental agitations (Fig. 1).

Despite the considerable work to date, the design and understanding of reconfigurable ensemble of NPs is still in its infancy. Currently employed reconfiguration strategies rely on modulating NP–NP interactions by rather brute-force methods including as solvent exchange and ligand transformation (e.g. heating or dynamic replacement of DNA molecules) [11–13]. Reconfiguration behaviors are explained in hindsight as much remains unknown about solvent-mediated NP-NP interactions; colloidal interactions at the nanoscale are nonadditive, subject to complicated multi-scale coupling effects [14]. Trial-and-error simulations were performed by iterating interaction potential forms until the results fit with experiments, making *a priori* design difficult [14]. New computational and experimental design routes which encode reconfigurability are needed for predictive engineering. A concurrent problem in that on the characterization side, it has been difficult to probe, in real time, the kinetic pathways of self-assembly and reconfiguration at the single NP level [14–18]. These pathways define how NPs arrange and rearrange into targeted structures [19]. Fully understanding the pathways requires real-space and in-situ characterization with high spatiotemporal resolution, which can capture the tumbling of NPs over their potential energy surface. Such data is inaccessible through existing ex-situ and ensemble characterization methods [20–25]. Small-angle X-ray scattering monitors the structure of NP self-assemblies in liquids, but only on the ensemble level [20–23]. Conventional transmission electron microscopy (TEM) resolves single

* Corresponding author at: Department of Materials Science and Engineering, University of Illinois, Urbana, IL 61801, United States.
E-mail address: qchen20@illinois.edu (Q. Chen).

https://doi.org/10.1016/j.cossms.2018.12.002
Received 30 July 2018; Received in revised form 5 December 2018; Accepted 14 December 2018

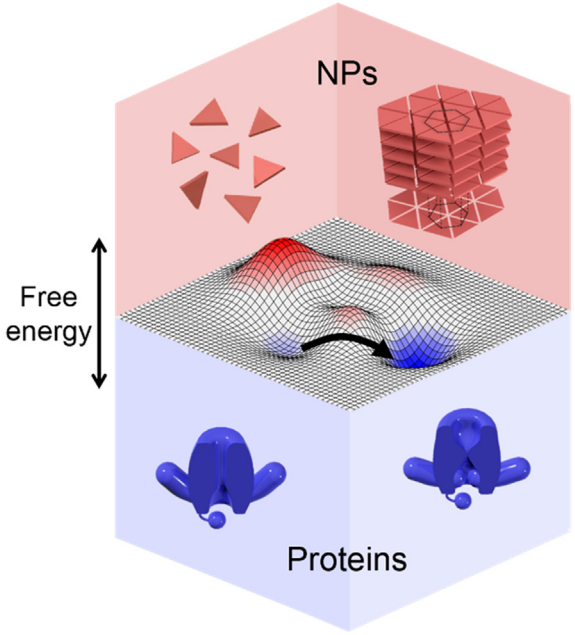

Fig. 1. The conceptual analogy between protein transformation (bottom: Ryanodine receptor opening and closing gates as an example) and the reconfiguration of NP ensembles (top: triangular prism NPs as an example) by a common multi-dimensional potential energy surface.

NPs, but are limited to dried or vitrified samples, not reconfiguring dynamics [24,25]. Nuclear magnetic resonance spectroscopy, though useful in studying biomolecular assembly, has been limited to probing surface ligands on NPs, and has not been suitable for NP assemblies due to large sample size [26,27]. The paucity of experimental data on the pathways, in return, hinders the validation of interaction models used in computation/theory and the establishment of rules for predictive design.

Here we discuss two aspects of progress in understanding and designing reconfigurable nanomaterials. The first is benefited by harnessing the recent advancements in liquid-phase TEM, which can directly image NP self-assembly and reconfiguration pathways [28–34]. To briefly introduce the method, liquid specimens are sandwiched and sealed between two electron-transparent windows for TEM imaging against high vacuum TEM operation condition [31]. The implementation of low-dose conditions in this method has shown to enable imaging with minimal beam effects (detailed discussions on beam effects in other review [16]) and generate experimental datasets that were inaccessible otherwise. One can obtain not only real-time and real-space evolution of NP ensembles in liquids, but also the response under stimuli at the single NP level. Mechanistic relations between NP building blocks and their nanoscale colloidal interactions can be derived to understand how they equilibrate into a final stable structure or interconvert among polymorphic states. The second is to highlight opportunities to design and engineer NP reconfigurability on various levels, such as employing shape-shifting building blocks and “smart” microfabricated platforms that are dynamic for NPs to reside upon. The vision is to integrate the emergent developments in other areas (e.g. polymer science, flexible electronics) and to enrich the design space for reconfigurability in structures, properties and applications, involving non-equilibrium dynamics.

2. Direct imaging of reconfiguration pathways by liquid-phase TEM

2.1. Step-growth “polymerization” of NPs

Liquid-phase TEM has the unique advantage to image and track motions of single NPs as they undergo reconfiguration, which allows quantitative comparison of their structural evolution to kinetic laws established in other scales. In particular, molecular polymerization, where many copies of reactive monomers are covalently linked into macromolecules, can be applicable to understand the assembly dynamics of NPs. The involved building blocks in both systems are self-repeating; they link directionally into complex architectures following their own coordination geometries. Moreover, recent work shows that the kinetics of structural formation in NPs can be explained by the quantitative rate equations for polymers, which predicts the molecular weight at a given synthesis condition.

This analogy was first corroborated in the case of gold nanorods assembling into chains [35]. The ensemble growth statistics monitored by stationary electron microscopy (EM) snapshots were found to follow step-growth polymerization, where bi- or multi-functional monomers react to form dimers, then longer oligomers and eventually chain polymers with one characteristic reaction constant (Fig. 2(a)). Recently, liquid-phase TEM work by Kim et al. [18] resolved the analogy through in-situ imaging, to elucidate fundamental real-time interactions and kinetic pathways from the single NP level. Gold triangular nanprisms of a side length of 90.9 ± 9.7 nm and a thickness of 7.5 nm were used as a prototypical system. The NP surface was coated by alkyl-thiol ligands terminated with $-COO^-$ groups, to render NPs electrostatically repulsive to each other. Self-assembly was triggered by screening this electrostatic repulsion and increasing the net NP-NP attraction. As shown in Fig. 2(b), liquid-phase TEM captured the process of the prisms attaching tip-to-tip, first into dimers, and finally into a distribution of chain-like assemblies (Fig. 2(b) and (c)). Statistical single NP tracking measures the length of all chains, x as the number of prisms (i.e. reactive “monomers”) in a chain, whose distribution shifts to higher values over time (Fig. 2(d)). From this distribution, number-averaged degree of polymerization ($\bar{X}_n$) was computed as an analog of molecular polymerization according to $\bar{X}_n = \sum n_x x / \sum n_x$, where n_x is the number of chains containing x NPs. As shown in Fig. 2(e), a linear relation of $\bar{X}_n$ to the assembly time t was found, quantitatively following the reaction-limited step-growth polymerization.

A constant k characterizing the rate of monomeric NP attachments can be extracted from the $\bar{X}_n - t$ fitting. In this system, it was measured to be 1.1×10^3 M^{-1} s^{-1} and stays constant as the chains grow, indicating that pairwise NP-NP interactions dominate the self-assembly. The rate constant, much like that in molecular reactions, can potentially serve as a quantitative characteristic to describe, compare and predict the driving force for NP self-assembly at various external conditions (e.g. pH, ionic strength, solvent polarity, temperature). For example, one potential conceptual extension can be deriving the activation energy in NP self-assembly by plugging in multiple rate constants measured in systematically-varying conditions into the Arrhenius equation. This activation energy, if tunable, can be engineered to enable other polymerization mechanisms in NP assembly, to develop exotic architectures (dendrimer, rings, hyperbranched polymer) and control their size/shape monodispersity (living polymerization). Fundamentally, the experimentally measurable rate constant can also be used as an input to validate and calibrate the time scales in dynamic simulations of NP assembly on potential energy surface, to facilitate the full predicting power of programmable reconfiguration behavior.

2.2. Colloidal interactions and reconfiguration pathways specific to the nanoscale

Unlike at micron-scale, where the convergence of real-space

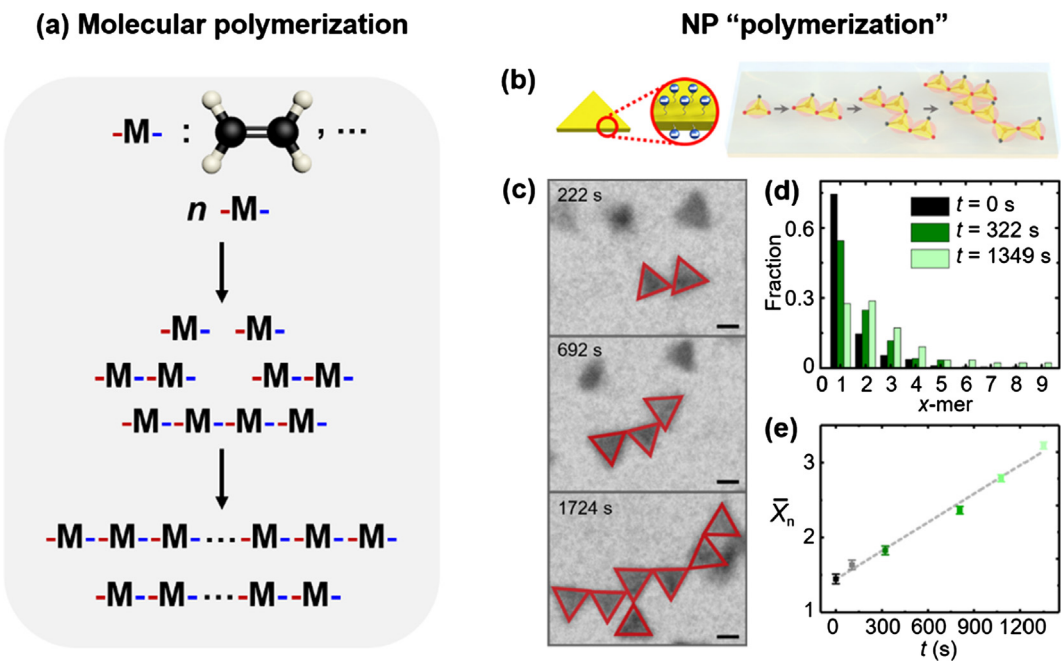

Fig. 2. Polymerization mechanisms of molecular monomers (a) and their NP analogues (b–e). (a) Schematics illustrating molecular step-growth polymerization where M stands for monomers with bi-functionality (blue and red bonds). (b) Gold triangular nanoprisms coated with negatively-charged thiols, which were observed to assemble into chains in the liquid-phase chamber for TEM imaging. (c) Time-lapse liquid-phase TEM images showing the tip-to-tip attachments of prisms into chains. (d) A graph showing the length (x) distribution of polymer-like NP chains at different time t. (e) A graph showing the linear growth of the number-averaged degree of polymerization over time calculated from in-situ observation of chain formation. (b)–(e) adapted from Ref. [18]. Scale bars: 50 nm.

imaging, microrheology, theory and modeling has enabled deep understandings [36–39], understandings of reconfiguration dynamics on the nanoscale, ubiquitous in geochemical, synthetic and biological systems, have remained elusive. The complication of fluctuations, solvent/ligand effects and the similarity between NP size and interaction range preclude direct translation of insights from micron-sized colloids (learned via optical microscopy imaging) to the nanoscale [40,41]. Liquid-phase TEM enables a paradigm shift by probing dynamic features intrinsic to the nanoscale. We discuss two aspects of colloidal interactions and reconfiguration pathways revealed by recent liquid-phase TEM work here, neither of which follows a simple rescaling of laws for micron-scale colloids: long-range interaction and nanoscale morphology effects. We expect more differences to emerge as more nanoscale reconfiguration pathways are thoroughly studied at the nanoscale. Just like how optical microscopy serves as the technical core for micron-sized colloids and cellular studies, the liquid-phase TEM imaging and analysis workflow here can establish a framework to explain the origin of greatly enriched phase states in nano-entities, which has generated exotic artificial materials forms such as quasi- [42], hierarchical [43,44] and clathrate [45] crystals as well as biological transformation such as protein folding [46] and DNA condensation [47].

2.2.1. *Long-range interaction effects*

Here long-range interaction effects refer to how NPs recognize each other way before they are in physical contact; the NP motion trajectories can thus be altered at a distance to adopt the most favorable approaching path. In comparison, for micron-sized colloids, their interaction ranges are two to three orders of magnitude smaller than their size, rendering negligible effects when they are apart. Take the prism self-assembly discussed above [18] as an example. When a pair of the prism NPs approach from a random initial separation (Fig. 3(a)), they follow traces which altogether select the tip-to-tip attachment (Fig. 3(c)). Based on the single NP position and orientation tracking (Fig. 3(a)), it has been found that a successful attachment occurs only when two prisms align tip-to-tip even a long distance apart (Fig. 3(c)). If the prisms attempt to come close side-by-side, they are mutually repelled away as soon as they are close than 10 nm distance, smartly rejecting the disfavored orientation at a distance. This long-range selection of assembly pathways agrees with the electrostatic repulsion profile computed between the two prisms (160 μM ionic strength). As shown in Fig. 3(b), the repulsion starts to take effect at a gap distance as large as 50 nm. The barrier for tip-to-tip (15 k_BT) approaching is smaller than that for side-by-side ($>$ 100 k_BT), favoring the former kinetic pathway to achieve 83% tip-to-tip connection in all the NP attachments of the system. Note that this pathway selection of final self-assembled structures can be utilized to overrun thermodynamically-favored ones, such as the non-closely packed NP chains observed here. The observed long-range effect among interacting nanoscale entities can be widely existing, like oriented attachment of crystallites into NPs [48], protein cooperativity in folding [49], and channel formation [50].

2.2.2. *Nanoscale morphology matters*

The nature of long-range NP-NP interactions renders the full shape details of interacting NPs crucial to understand the reconfiguration pathways, while micron-sized colloids concern merely local surface area when external fields are not present due to the relatively short interaction range [51,52]. As a result, morphology details of NPs, which can be as small as a few nanometers and thus, often regarded as trivial, become critical in manipulating the types of structures that NPs form into. For example, simple triangular prism NPs can have distinct geometric details (Fig. 4). For the Mirkin prisms [21] denoted as prism 1, direct high-resolution TEM imaging and spatial map of the local surface curvature revealed that the tips of the triangular prisms are either round or flat (Fig. 4(a)), which directs the connection "bond angle" between two neighboring NPs in a chain to a bimodal distribution [18]. Instead forming into a perfect bowtie (0° bond angle) when both tips are round, the other sawtooth motif of a 60° bond angle occurs when one of the tips is flat (Fig. 4(b)). Theoretical modeling of the net NP-NP interaction (E_{tot}) quantitatively correlating the bond angle with the morphology of prism tips agrees with the experiments. As shown in Fig. 4(c), the local surface curvature of prism tips fine-tunes the balance

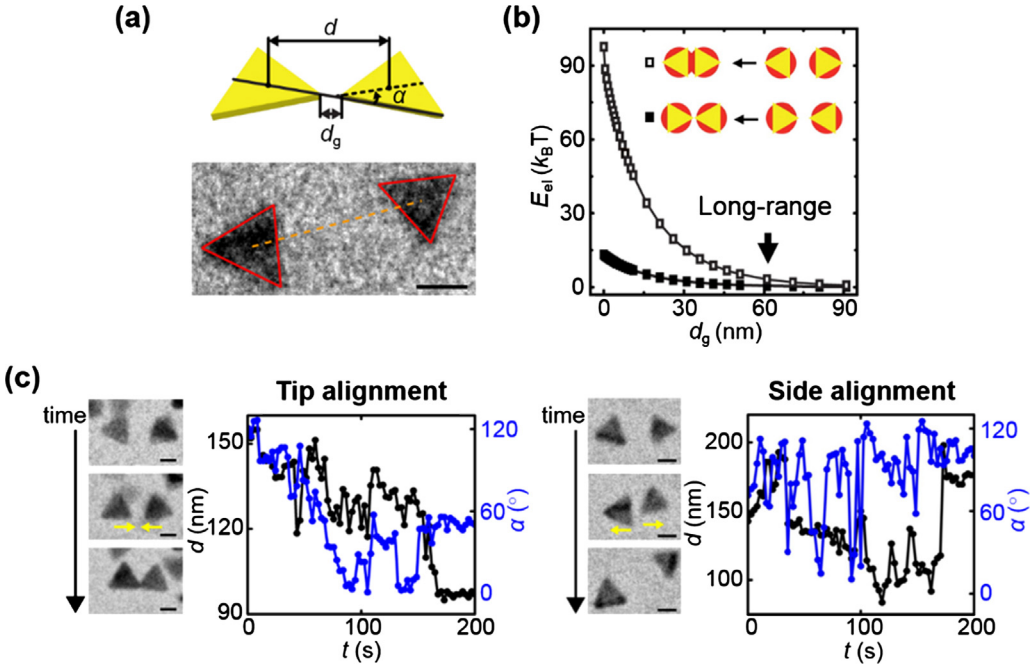

Fig. 3. Approaching traces of a NP pair due to a long-range electrostatic repulsion (adapted from Ref. [18]). (a) Parameterization of traces for anisotropically-shaped NPs (triangular nanoprisms here, top) and a typical TEM image with contour tracking (bottom). (b) Computed electrostatic repulsion E_{el} of two prisms approaching in tip-to-tip (filled-square) and side-by-side (open square) configurations. (c) Representative traces of the two approaching prisms, including time-lapse liquid-phase TEM images and the corresponding graphs of distance d (black filled circles) and relative orientation α (blue filled circle) as a function of t. Scale bars: 50 nm in (a) and (c). (For interpretation of the references to colour in this figure legend, the reader is referred to the web version of this article.)

of van der Waals attraction and electrostatic repulsion to vary the most favored bond angle as well as the final assembled structure. For prism 2 synthesized following a seedless growth, they have the interesting detail of beveled sides [53], where their sides convexly enclosed by two flat surfaces as shown in Fig. 4(d). This fine feature garnered reconfiguring ensemble structures as surfactant concentration changes, and a novel interlocked honeycomb lattice at high depletion attraction (Fig. 4(e) and (f)) as the densest packing. This interlocked lattices pack more densely than the conventional planar honeycomb lattice, which greatly enhances the plasmonic coupling with a 5-fold increase in the surface-enhanced Raman scattering. The importance of the nanomorphology can be switched on and off to create polymorphic states and introduce versatility in structural manipulation, which can be further utilized as a robust method to guide the nanoscale building blocks into one final state over the other. Such switchability provides design space for developing materials with great performance in response to external environments.

The crucial role of nanoscale morphology highlights the potency of real-space, high resolution imaging of NP assembly using liquid-phase TEM, which in return provides inputs for computational study in

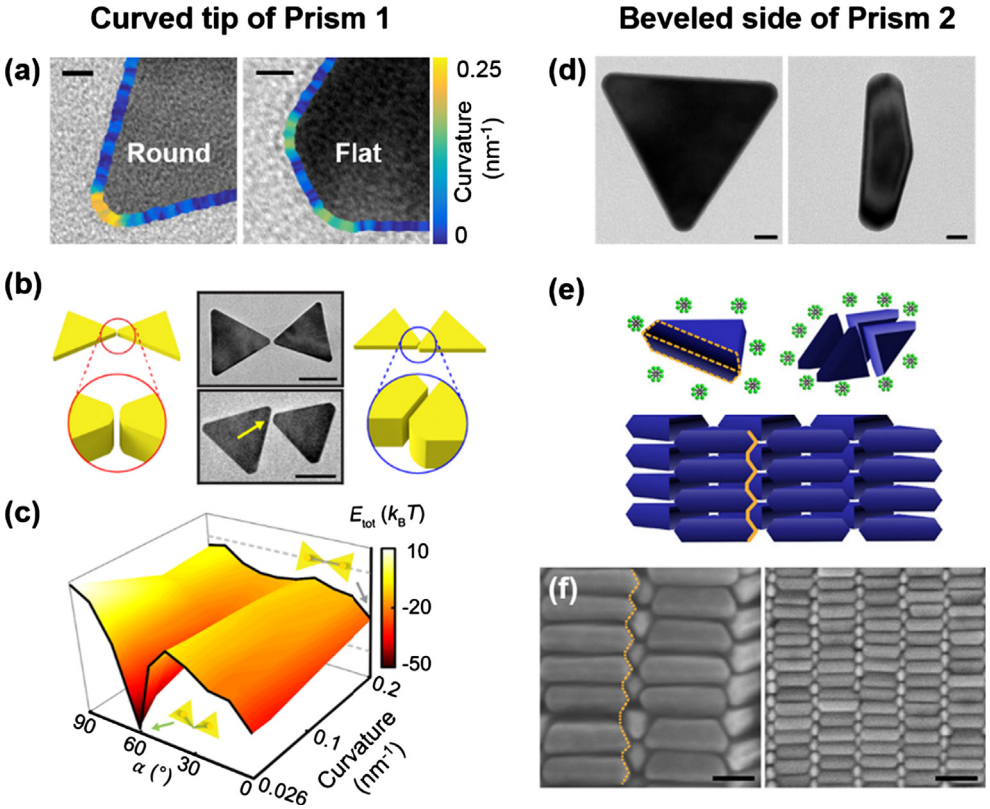

Fig. 4. The role of the nontrivial nanoscale morphology in NPs. (a) TEM images of the prism tips with the contour lines color-coded to local surface curvature. (b) TEM images and schematics of dimers in bowtie (0° bond angle, top) and sawtooth (60° bond angle, bottom) bonding motifs. (c) A graph showing the net pairwise prism interaction E_{tot} as a function of bond angle and tip flatness. (a)–(c): adapted from Ref. [18]. (d) TEM images of the beveled gold triangular NPs. (e) Schematics of the beveled gold prisms and the self-assembled interlocked honeycomb lattice (SEM in (f)) under depletion attraction. (d)–(f) adapted with permission from Ref. [53]. Copyright 2017 American Chemical Society. Scale bars: (a) 5 nm; (b) 30 nm; (d) 5 nm; (f) 40 nm (left), 100 nm (right).

pushing the boundaries of mechanistic understanding. In the case of prisms with curved tips (Fig. 4(c)), the prism tip shape was constructed from spheres of sizes of a gold atom to fully represent that observed in TEM [18], which gives precise NP-NP interaction profile. For other nano-entity systems, it remains a general challenge to balance between detailed morphology modeling and appropriate coarse-graining to minimize computation time. A close-knit feedback loop between liquid-phase TEM observations and computational modeling can potentially resolve the challenge and lead to comprehending the fundamental self-configuration rules at the nanoscale in liquids.

2.3. In-situ triggering of reconfiguration in solution

Besides direct imaging, liquid-phase TEM enables modulation of NP-NP interactions which can trigger in-situ structural reconfiguration. Using the one-dimensional lamellar structure stacked face-to-face by gold triangular nanoprisms as an example, Kim et al. captured how the lattice constant of the assembly changes upon a local ionic strength variation in liquid-phase TEM [17]. The reconfiguration of ensemble structure took only minutes to complete, offering us the sense of time-scale for NPs to collectively sample the possible states on the energy surface by repositioning and arriving at the most favorable state. While this reconfiguration still maintains the lamellar symmetry of the original lattice, in the lateral assembly of gold NPs discussed in Section 2.1, the topology of the final assemblies was tuned from linear chains to networked chains. As the ionic strength increases (205 μM), the NP-NP electrostatic repulsion was screened to expose all the three tips of one prism as reactive, namely of a valency increased from 2 to 3 (Fig. 5(a)), and "polymerize" into cross-linked networks (Fig. 5(b)). Fig. 5(c) shows finite-difference-time-domain (FDTD) calculations for the as-assembled linear and networked chains. The spatial pattern of locally enhanced electric fields changes as the topology and the number of tip-to-tip connection vary with ionic strength, implicating the potential of engineering an active nanoantenna array [54] and near-field illumination resources for imaging [55] and energy conversion [56]. Additionally, one can achieve other types of concurrent real-time imaging and structural modulation in solution under liquid-phase TEM, by introducing liquid flow, heating, electric stimulation and even light illumination [16].

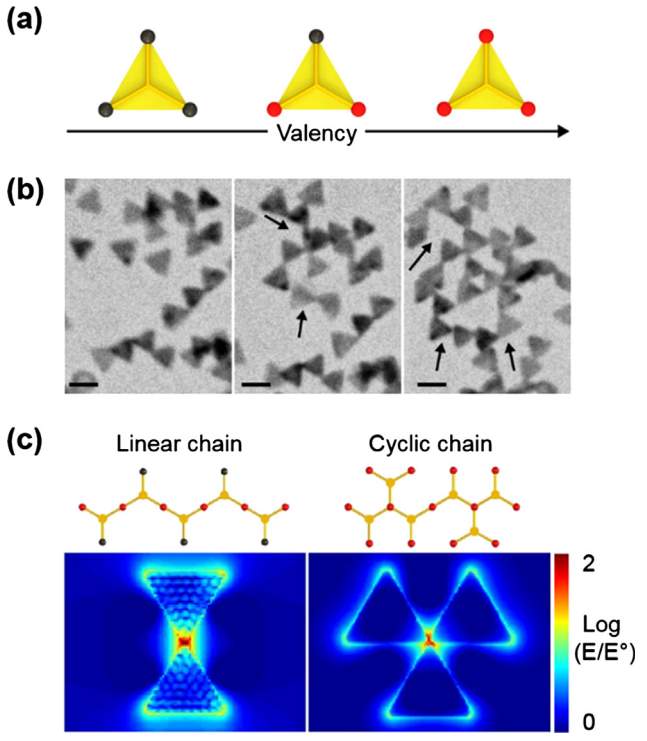

Fig. 5. In-situ control of NP bonding geometry. (a) Schematics showing the adaptive bonding geometry of the prisms. The red dots are the reactive sites that determine the connection scheme and final assembly structure. (b) Time-lapse liquid-phase TEM images of the assembly of triangular prisms into cyclic chains. Black arrows show the direction of assembly. (c) FDTD calculations on the linear and cyclic chains. (a) and (b) adapted from Ref. [18]. Scale bars: 100 nm.

2.4. Correlating liquid-phase TEM studies with computer simulation

The fast development in simulation techniques and energy landscape sampling methods has been greatly useful in colloidal studies, from predicting the spontaneous organization of active colloids [57,58] to gaining physical insights into phenomena such as glass transition [59] and nonclassical crystallization pathways [37]. Computer simulations can probe huge design space such as particle shapes [40], size polydispersity [37], external field [58,60], and interparticle interactions more easily than experiments to study their influence on the colloidal behaviors [61]. For differently-shaped nanoparticles [5,14], simulations have been successfully applied in multiple self-assembly studies to gain insights into the kinetic pathways. For example, simulations have helped clarify the complex clathrate crystal structure assembled by DNA coated gold bipyramids [45], understand the mechanism of experimentally-observed self-assembly, such as the quasicrystal formed from binary nanospheres [42], and self-limited growth of polydispersed nanoparticles into assembled monodispersed supraspheres [44].

Meanwhile, there are complications associated with these simulation studies. The physical driving forces for self-assembly, i.e. interactions between nanoparticles, depend sensitively on the fine details of nanoparticle shapes. They are more complex to model than the interactions of micron-sized colloidal particles due to non-additivity and multi-coupling effects as discussed in previous literature [14,62]. Simulating anisotropic, especially nonconvex, shapes is more difficult compared with convex geometries [63]. And most importantly, the kinetic pathways demonstrated in dynamics simulation used to be difficult to be experimentally verified before the advent of liquid-phase TEM. We see great opportunities emerging from integration of simulation methods with liquid-phase TEM studies. For example, the nanoparticle interactions experimentally mapped in liquid-phase TEM can serve as input parameters for simulation and further predict new assembly structures. Liquid-phase TEM can capture the structures of precursors or transient intermediates towards the final assembly, which can be used as comparison and calibration with assembly trajectories observed in simulations to enable correct predictions of assembly behaviors. It is noteworthy that liquid-phase TEM experiments can involve the effects from the electron beam [17,64] and the sandwiching geometry of liquid chamber [18,65], which are attracting increasing mechanistic understandings (see focused reviews [16,31]). For example, several gold nanoparticle assembly work showed that when the electron dose rate is low ($< 30\ e^{-}\cdot Å^{-2}\cdot s^{-1}$), the beam induces an effective ionic strength increase [17,18,66] that directs the assembly through screening of electrostatic repulsion.

3. Emergent strategies for reconfiguration at the nanoscale

3.1. Shape-shifting colloids

While the examples above are mostly on the assembly and reconfiguration of unchanging NPs, the design space of reconfigurable nanomaterials can be pushed to complex NPs that are "dynamically" reconfigurable – the NP shape shifts upon external stimulus. Such "dynamic" building blocks—not fixed, but adaptive to an external stimulus—can add another level of reconfigurability to NP ensembles, moving towards systems that adapt structures and functions fully from

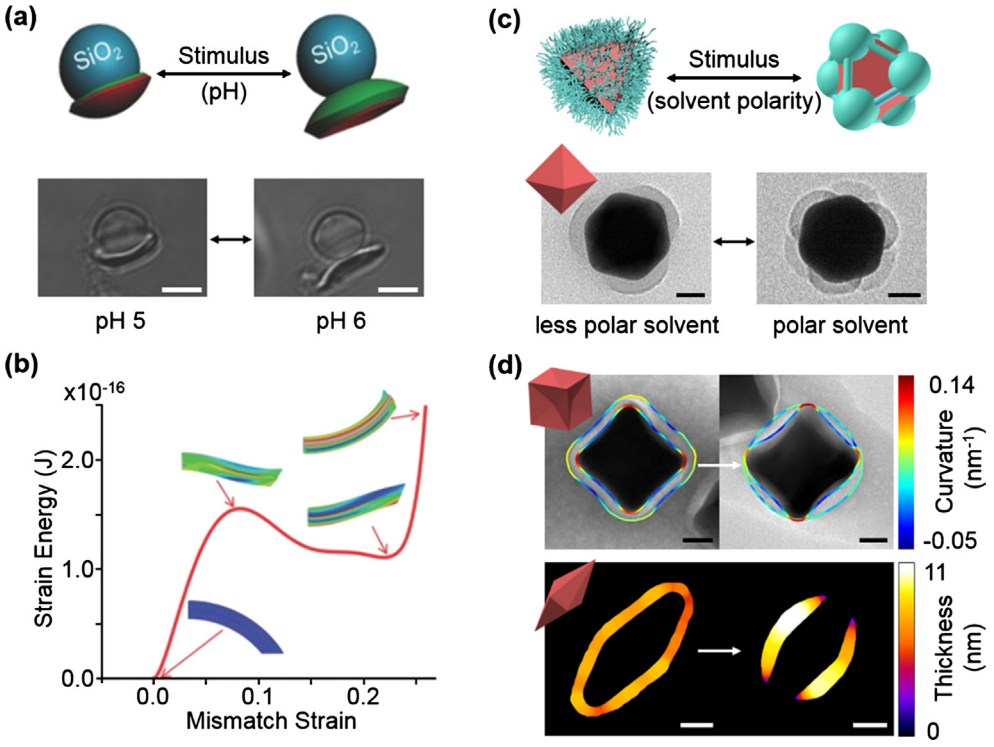

Fig. 6. Shape-shifting colloids. (a) Schematics and optical microscopy images of the shape transformation of the layered polymer coating on a silica core triggered by pH changes. (b) A graph of predicted bistability plot for the snap-buckling colloids based on finite element analysis. (c) Schematics (top) and TEM images (bottom) of PS-shelled octahedral NPs during a phase segregation. (d) TEM images of PS-shelled concave cube NPs before and after phase segregation with the contour lines of the polymer shell colored by local curvature values. The same observation with bipyramid NPs was shown and colored by local thickness values. Scale bars: (a) 4 μm; (c), (d) 20 nm. (a) and (b) used with permission from Ref. [72]. Copyright 2015 Wiley; (c) and (d) used with permission from Ref. [73]. Copyright 2018 Wiley. (For interpretation of the references to colour in this figure legend, the reader is referred to the web version of this article.)

bottom-up. So far simulations have taken the lead in implementing the strategy and studying how superlattices assembled from NPs adapt as individual NPs undergo a shape change [67,68]. Either first-order or second-order solid-to-solid transitions can be triggered depending on the shape shifting pathways of component NPs. For example, for NPs with hard-core interactions, a first-order phase transition was observed for face centered cubic to body-centered cubic (BCC) transition while a continuous phase transition was observed for the phase transition from BCC to simple cubic [68].

Experimental realization of shape-shifting colloids has been focused extensively on polymeric micron-sized colloids [69–71], as most synthetic NPs are inorganic and nondeformable. A promising novel strategy to implement shape-shifting in NPs is to integrate inorganic, static-shape NP core with deformable polymeric materials. Epstein et al. demonstrated this hybridizing strategy in micron-sized colloids. They designed pH-responsive micron-sized colloids rapidly switching (< 200 ms) between two mechanically bistable shapes [72]. As shown in Fig. 6(a), two layers of polymers were deposited onto an inorganic SiO_2 core: the first layer is poly(acrylic acid) (PAA) hydrogel ($pK_a \approx 4.7$), which expands as pH increases; the second is poly(vinyl cinnamate) (PVCi) organogel, insensitive to pH. The polymers tethered to the silica core stay as the original shape at low pH (< 5), but immediately flip outwards as PAA swells at higher pH (> 6). From finite element analysis and direct microscopy imaging, the actuation was found to occur in a three-step process: a continuous deformation of the polymer layers upon a pH increase, a drastic "snap-buckling" of polymer layer from a positive curvature to a negative one, finally a gradual relaxation to the final stable configuration (Fig. 6(a) and (b)). Such stress application to crosslinked polymers (which exhibit certain degrees of rigidity) coated on inorganic cores by external triggers such as pH, ionic strength, magnetic and electric actuation can often change the colloidal shape abruptly and reversibly in a controllable way, potentially generalizable to inorganic NPs.

In addition to actuating cross-linked polymers all at once as a whole, phase segregation of polymer chains on NPs can also provide a valuable knob not only in engineering the shape-shifting behavior, but also in utilizing the geometric shape of NPs. Kim et al. reported the segregation of grafted polymer layers coated on a variety of anisotropic NP cores (e.g. cube, octahedron, concave cube, bipyramid) [73] and quantitatively analyzed how the reconfiguration of polymer shells varied with the core NP shape. Before segregation, both polystyrene (PS) and polystyrene-*b*-poly(acrylic acid) (PS-*b*-PAA) shells were shown uniformly coated on gold NP surfaces by gold-thiol bond either directly or indirectly adhered to the polymers. Then the polymer segregation occurs either through a solvent polarity (PS-tethered NPs) or temperature change (PS-*b*-PAA coated NPs), which was characterized by the shell contour analysis on local curvature and thickness. The result showed PS shells locally thicken at high curvature regions (vertices and edges), while the PS-*b*-PAA shells segregate to the flat facets (Fig. 6(c) and (d)), demonstrating complementary "patchy" patterns of polymers on the NPs. Harnessing these two distinct trends together can be very helpful in pushing forward our anticipation for achieving comprehensive functional assembly with manipulatable phase behavior of NPs continuously changing their morphology. The vision is that when many of such NPs interact with each other, their capability to undergo transitions from a uniform polymer coating to a patchy one can immediately change the interaction profile of the NPs and trigger a collective reconfiguration process. There is a great potential in studying the relationship among the external stimuli, the shape change of a single NP, and the propagation of the change from one single component NP to the NP ensemble with recent experimental capabilities, which can pave the way for innovative applications with desired performance that one can hardly predict as of now.

3.2. *Reconfigurable and redefinable platforms for colloidal self-assembly*

The last emergent reconfiguration strategy is to trigger the reconfiguration of NP arrangement by actuating the substrate they reside upon, which can be integrated with a wide range of functional platforms used in practical devices. Such reconfigurable platforms build on recent advancements in flexible and stretchable electronics, where electronic circuits or photonic devices patterned on a 2D substrate by conventional microfabrication can be actuated to form a 3D structure (chiral pedal, knots, etc.) due to a compressive buckling or tension

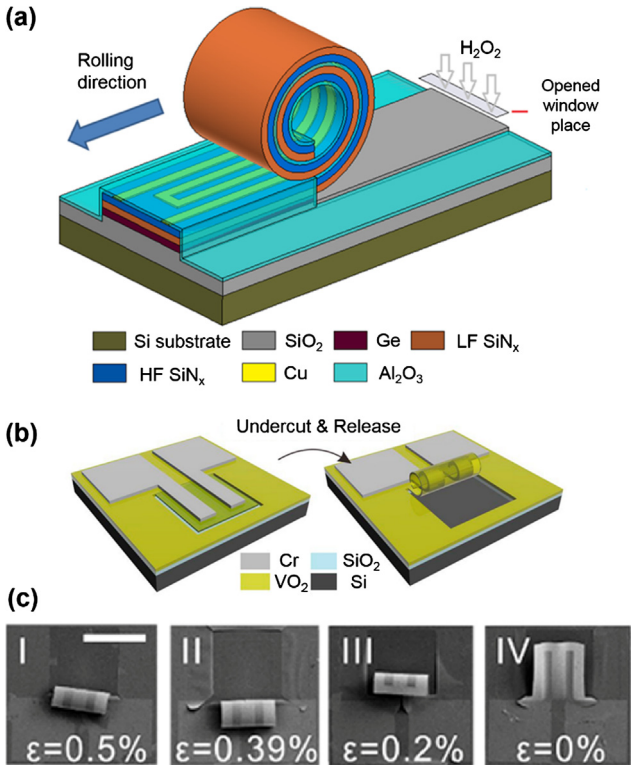

Fig. 7. Reconfigurable and redefinable SRuM platforms fabricated using a top-down approach which can serve as emerging platforms for colloidal assembly. (a) Schematic illustration of SiN_x SRuM platform used for inductor design. (b) Schematic illustration of the structure and fabrication process of the Cr/VO_2 SRuM architecture. (c) SEM images of VO_2 SRuM structures with different amount of strain as indicated, used for reversible rolling. Scale bar: (c) 100 μm. (a) reprinted with permission from Ref. [83]. Copyright 2017 IEEE; (b) and (c) adapted with permission from Ref. [87]. Copyright 2018 American Chemical Society.

mismatch in the circuit layers as [74–80]. This structure transformation can be modelled accurately for reverse design, providing a versatile, precisely-designed dynamic platform. The flexible substrate can serve as a platform upon which colloidal assemblies reside, much like how a chemically patterned substrate was used to direct locally concentrated colloidal packing [81], yet with the key advancement to enable reconfiguration compatible with NPs of different materials and assembly structure. For example, Huang et al. designed and fabricated a platform of Self-Rolled-Up Membranes (SRuMs) by coating sequentially sacrificial, low-frequency SiN_x and high-frequency SiN_x layers on a silicon substrate [76]. Due to the strain mismatch between the two SiN_x layers, the membrane can roll up after etching the sacrificial layer away. This platform alone can be used for many purposes, such as miniaturized inductors/transformers as shown in Fig. 7(a) [82–84] or a platform for controlling the growth of neuron cells [85]. The incorporation of bottom-up colloidal self-assembly to this top-down platform will open a new door for designing ultimate reconfigurable system with various potential usage. One can expect to immediately bridge colloidal science and device engineering by depositing magnetic, conducting, or semiconducting NP assemblies onto SRuMs. One demonstration has been recently reported on loading branched metal-organic framework (MOF) colloids onto SRuMs [86]. Furthermore, transforming a 2D-assembled structure into 3D can not only bring hybrid functionalities inaccessible by a 2D material, also deepen our understanding in geometry and chemistry of substrate effect at the nanoscale.

The 3D tubular microstructure of the SRuMs can be redefinable as long as the strain of the as-grown nanomembrane can be further tuned after the completely rolled-up process. In a recent study, a VO_2 nanomembrane based architecture was demonstrated to achieve reversible rolling by controlling the phase transition temperatures of VO_2, which provides a promising way for redefinable colloidal self-assembly [87]. As shown in Fig. 7(b) and (c), unlike the SiN_x SRuM platform discussed above, the strain mismatch to generate sufficient bending energy comes from the internal stress gradient of VO_2 nanomembrane during the thinning process. The internal strain can be enhanced by a patterned chromium (Cr) layer deposited on top of the VO_2 nanomembrane, which serves as the electrodes. By applying direct current on the two electrodes to establish static electric field, current goes across the VO_2 nanomembrane and generates joule heating to increase its temperature. Once the temperature hits the transition point, internal strain of VO_2 nanomembrane changes triggering reversible rolling. Utilizing this novel SRuM platform, colloidal self-assembly incorporation can be further reconfigured and interconvert among multiple states. All the rolled-up parameters such as number of turns and inner diameter could be redefined by convenient external electrical signal control.

4. Outlook

The long-term perspective of interpreting and engineering nanoscale reconfigurable materials is to discover, understand, and implement the rules to make artificial materials exhibit functional features of living systems (e.g. adaptive and evolving, not static matter). Though explored for larger building blocks (1–100 μm), the potential opportunities emerging from active materials at the nanoscale are just starting to gain significant attention. Quantifying the building block-nanoscale interaction-targeted structure relationship will pave the foundation for future work: applying the principles learned to engineer the kinetic pathways taken to a final structure, both in silico and in lab, and to program functions that change on demand. Application-wise, these structures can be further tested and optimized into reconfigurable devices that mimic living matter. Moreover, based on the testbed NP system, the imaging, analysis techniques as well as design principles can be extended to other objects (e.g. proteins, polymer micelles), to develop a diverse library of materials and transfer concepts to corresponding disciplines, such as biophysics, polymer physics, and non-equilibrium statistical mechanics.

Acknowledgements

This work was supported by the U.S. Department of Energy, Office of Basic Energy Sciences, Division of Materials Sciences and Engineering under Award No. DE-FG02-07ER46471, through the Materials Research Laboratory at the University of Illinois.

Appendix A. Supplementary material

Supplementary data associated with this article can be found, in the online version, at https://doi.org/10.1016/j.cossms.2018.12.002.

References

[1] S.C. Glotzer, Assembly engineering: materials design for the 21st century (2013 P.V. Danckwerts lecture), Chem. Eng. Sci. 121 (2015) 3–9.
[2] L. Phan, W.G. Walkup, D.D. Ordinario, E. Karshalev, J.-M. Jocson, A.M. Burke, A.A. Gorodetsky, Reconfigurable infrared camouflage coatings from a cephalopod protein, Adv. Mater. 25 (39) (2013) 5621–5625.
[3] J.C. Nawroth, H. Lee, A.W. Feinberg, C.M. Ripplinger, M.L. McCain, A. Grosberg, J.O. Dabiri, K.K. Parker, A tissue-engineered jellyfish with biomimetic propulsion, Nat. Biotechnol. 30 (2012) 792.
[4] S.-J. Park, M. Gazzola, K.S. Park, S. Park, V. Di Santo, E.L. Blevins, J.U. Lind, P.H. Campbell, S. Dauth, A.K. Capulli, F.S. Pasqualini, S. Ahn, A. Cho, H. Yuan, B.M. Maoz, R. Vijaykumar, J.-W. Choi, K. Deisseroth, G.V. Lauder, L. Mahadevan, K.K. Parker, Phototactic guidance of a tissue-engineered soft-robotic ray, Science 353 (6295) (2016) 158–162.
[5] M.A. Boles, M. Engel, D.V. Talapin, Self-assembly of colloidal nanocrystals: from intricate structures to functional materials, Chem. Rev. 116 (18) (2016)

11220–11289.
[6] A.F. Smith, R.G. Weiner, S.E. Skrabalak, Symmetry-dependent optical properties of stellated nanocrystals, J. Phys. Chem. C 120 (37) (2016) 20563–20571.
[7] D.V. Talapin, J.-S. Lee, M.V. Kovalenko, E.V. Shevchenko, Prospects of colloidal nanocrystals for electronic and optoelectronic applications, Chem. Rev. 110 (1) (2010) 389–458.
[8] C.R. Kagan, E. Lifshitz, E.H. Sargent, D.V. Talapin, Building devices from colloidal quantum dots, Science 353 (6302) (2016) aac5523.
[9] J. Zhu, M.C. Hersam, Assembly and electronic applications of colloidal nanomaterials, Adv. Mater. 29 (4) (2017) 1603895.
[10] N. Jiang, X. Zhuo, J. Wang, Active plasmonics: principles, structures, and applications, Chem. Rev. 118 (6) (2018) 3054–3099.
[11] M.R. Jones, N.C. Seeman, C.A. Mirkin, Programmable materials and the nature of the DNA bond, Science 347 (6224) (2015) 1260901.
[12] Y. Kim, R.J. Macfarlane, M.R. Jones, C.A. Mirkin, Transmutable nanoparticles with reconfigurable surface ligands, Science 351 (6273) (2016) 579–582.
[13] J.A. Mason, C.R. Laramy, C.-T. Lai, M.N. O'Brien, Q.-Y. Lin, V.P. Dravid, G.C. Schatz, C.A. Mirkin, Contraction and expansion of stimuli-responsive DNA bonds in flexible colloidal crystals, J. Am. Chem. Soc. 138 (28) (2016) 8722–8725.
[14] C.A. Silvera Batista, R.G. Larson, N.A. Kotov, Nonadditivity of nanoparticle interactions, Science 350 (6257) (2015) 1242477.
[15] O. Gang, Nanoparticle assembly: from fundamentals to applications: concluding remarks, Faraday Discuss. 186 (2016) 529–537.
[16] B. Luo, J.W. Smith, Z. Ou, Q. Chen, Quantifying the self-assembly behavior of anisotropic nanoparticles using liquid-phase transmission electron microscopy, Acc. Chem. Res. 50 (5) (2017) 1125–1133.
[17] J. Kim, M.R. Jones, Z. Ou, Q. Chen, In situ electron microscopy imaging and quantitative structural modulation of nanoparticle superlattices, ACS Nano 10 (11) (2016) 9801–9808.
[18] J. Kim, Z. Ou, M.R. Jones, X. Song, Q. Chen, Imaging the polymerization of multivalent nanoparticles in solution, Nat. Commun. 8 (1) (2017) 761. This work is licensed under the Creative Commons Attribution 4.0 International License. To view a copy of this license, visit http://creativecommons.org/licenses/by/4.0/.
[19] J.J. De Yoreo, P.U.P.A. Gilbert, N.A.J.M. Sommerdijk, R.L. Penn, S. Whitelam, D. Joester, H. Zhang, J.D. Rimer, A. Navrotsky, J.F. Banfield, A.F. Wallace, F.M. Michel, F.C. Meldrum, H. Cölfen, P.M. Dove, Crystallization by particle attachment in synthetic, biogenic, and geologic environments, Science 349 (6247) (2015) aaa6760.
[20] W. Cheng, M.R. Hartman, D.-M. Smilgies, R. Long, M.J. Campolongo, R. Li, K. Sekar, C.-Y. Hui, D. Luo, Probing in real time the soft crystallization of DNA-capped nanoparticles, Angew. Chem., Int. Ed. 49 (2) (2010) 380–384.
[21] K.L. Young, M.R. Jones, J. Zhang, R.J. Macfarlane, R. Esquivel-Sirvent, R.J. Nap, J. Wu, G.C. Schatz, B. Lee, C.A. Mirkin, Assembly of reconfigurable one-dimensional colloidal superlattices due to a synergy of fundamental nanoscale forces, Proc. Natl. Acad. Sci. USA 109 (7) (2012) 2240–2245.
[22] M.C. Weidman, D.-M. Smilgies, W.A. Tisdale, Kinetics of the self-assembly of nanocrystal superlattices measured by real-time in situ X-ray scattering, Nat. Mater. 15 (2016) 775.
[23] T. Li, A.J. Senesi, B. Lee, Small angle X-ray scattering for nanoparticle research, Chem. Rev. 116 (18) (2016) 11128–11180.
[24] A. Durand, G. Papai, P. Schultz, Structure, assembly and dynamics of macromolecular complexes by single particle cryo-electron microscopy, J. Nanobiotechnol. 11 (1) (2013) S4.
[25] J. Frank, Story in a sample—the potential (and limitations) of cryo-electron microscopy applied to molecular machines, Biopolymers 99 (11) (2013) 832–836.
[26] L.E. Marbella, J.E. Millstone, NMR techniques for noble metal nanoparticles, Chem. Mater. 27 (8) (2015) 2721–2739.
[27] A. Badia, R.B. Lennox, L. Reven, A dynamic view of self-assembled monolayers, Acc. Chem. Res. 33 (7) (2000) 475–481.
[28] N. de Jonge, F.M. Ross, Electron microscopy of specimens in liquid, Nat. Nanotechnol. 6 (2011) 695.
[29] E.A. Lewis, S.J. Haigh, T.J.A. Slater, Z. He, M.A. Kulzick, M.G. Burke, N.J. Zaluzec, Real-time imaging and local elemental analysis of nanostructures in liquids, Chem. Commun. 50 (70) (2014) 10019–10022.
[30] T. Ngo, H. Yang, Toward ending the guessing game: study of the formation of nanostructures using in situ liquid transmission electron microscopy, J. Phys. Chem. Lett. 6 (24) (2015) 5051–5061.
[31] F.M. Ross, Opportunities and challenges in liquid cell electron microscopy, Science 350 (6267) (2015) aaa9886.
[32] J.J. De Yoreo, N.A. Sommerdijk, Investigating materials formation with liquid-phase and cryogenic TEM, Nat. Rev. Mater. 1 (2016) 16035.
[33] H.-G. Liao, H. Zheng, Liquid cell transmission electron microscopy, Annu. Rev. Phys. Chem. 67 (1) (2016) 719–747.
[34] H.-W. Lee, Y. Li, Y. Cui, Perspectives in in situ transmission electron microscopy studies on lithium battery electrodes, Curr. Opin. Chem. Eng. 12 (2016) 37–43.
[35] K. Liu, Z. Nie, N. Zhao, W. Li, M. Rubinstein, E. Kumacheva, Step-growth polymerization of inorganic nanoparticles, Science 329 (5988) (2010) 197–200.
[36] B. Li, D. Zhou, Y. Han, Assembly and phase transitions of colloidal crystals, Nat. Rev. Mater. 1 (2016) 15011.
[37] T. Palberg, Crystallization kinetics of colloidal model suspensions: recent achievements and new perspectives, J. Phys. Condens. Matter 26 (33) (2014) 333101.
[38] Z. Wang, F. Wang, Y. Peng, Z. Zheng, Y. Han, Imaging the homogeneous nucleation during the melting of superheated colloidal crystals, Science 338 (6103) (2012) 87–90.
[39] Z. Wang, F. Wang, Y. Peng, Y. Han, Direct observation of liquid nucleus growth in homogeneous melting of colloidal crystals, Nat. Commun. 6 (2015) 6942.
[40] P.F. Damasceno, M. Engel, S.C. Glotzer, Predictive self-assembly of polyhedra into complex structures, Science 337 (6093) (2012) 453–457.
[41] U. Agarwal, F.A. Escobedo, Mesophase behaviour of polyhedral particles, Nat. Mater. 10 (2011) 230.
[42] X. Ye, J. Chen, M. Eric Irrgang, M. Engel, A. Dong, Sharon C. Glotzer, C.B. Murray, Quasicrystalline nanocrystal superlattice with partial matching rules, Nat. Mater. 16 (2016) 214.
[43] K. Miszta, J. de Graaf, G. Bertoni, D. Dorfs, R. Brescia, S. Marras, L. Ceseracciu, R. Cingolani, R. van Roij, M. Dijkstra, L. Manna, Hierarchical self-assembly of suspended branched colloidal nanocrystals into superlattice structures, Nat. Mater. 10 (2011) 872.
[44] Y. Xia, T.D. Nguyen, M. Yang, B. Lee, A. Santos, P. Podsiadlo, Z. Tang, S.C. Glotzer, N.A. Kotov, Self-assembly of self-limiting monodisperse supraparticles from polydisperse nanoparticles, Nat. Nano 6 (2011) 580.
[45] H. Lin, S. Lee, L. Sun, M. Spellings, M. Engel, S.C. Glotzer, C.A. Mirkin, Clathrate colloidal crystals, Science 355 (6328) (2017) 931–935.
[46] K.A. Dill, J.L. MacCallum, The protein-folding problem, 50 years on, Science 338 (6110) (2012) 1042–1046.
[47] V.B. Teif, K. Bohinc, Condensed DNA: condensing the concepts, Prog. Biophys. Mol. Biol. 105 (3) (2011) 208–222.
[48] A.P. Alivisatos, Naturally aligned nanocrystals, Science 289 (5480) (2000) 736–737.
[49] K.A. Dill, K.M. Fiebig, H.S. Chan, Cooperativity in protein-folding kinetics, Proc. Natl. Acad. Sci. USA 90 (5) (1993) 1942–1946.
[50] G. Dahl, R. Azarnia, R. Werner, Induction of cell–cell channel formation by mRNA, Nature 289 (1981) 683.
[51] J.R. Savage, D.W. Blair, A.J. Levine, R.A. Guyer, A.D. Dinsmore, Imaging the sublimation dynamics of colloidal crystallites, Science 314 (5800) (2006) 795–798.
[52] S. Sacanna, W.T.M. Irvine, P.M. Chaikin, D.J. Pine, Lock and key colloids, Nature 464 (2010) 575.
[53] J. Kim, X. Song, F. Ji, B. Luo, N.F. Ice, Q. Liu, Q. Zhang, Q. Chen, Polymorphic assembly from beveled gold triangular nanoprisms, Nano Lett. 17 (5) (2017) 3270–3275.
[54] M.W. Knight, H. Sobhani, P. Nordlander, N.J. Halas, Photodetection with active optical antennas, Science 332 (6030) (2011) 702–704.
[55] N. Fang, H. Lee, C. Sun, X. Zhang, Sub-diffraction-limited optical imaging with a silver superlens, Science 308 (5721) (2005) 534–537.
[56] S. Linic, P. Christopher, D.B. Ingram, Plasmonic-metal nanostructures for efficient conversion of solar to chemical energy, Nat. Mater. 10 (2011) 911.
[57] M.C. Marchetti, J.F. Joanny, S. Ramaswamy, T.B. Liverpool, J. Prost, M. Rao, R.A. Simha, Hydrodynamics of soft active matter, Rev. Mod. Phys. 85 (3) (2013) 1143–1189.
[58] J. Yan, M. Han, J. Zhang, C. Xu, E. Luijten, S. Granick, Reconfiguring active particles by electrostatic imbalance, Nat. Mater. 15 (2016) 1095.
[59] L. Berthier, G. Biroli, Theoretical perspective on the glass transition and amorphous materials, Rev. Mod. Phys. 83 (2) (2011) 587–645.
[60] J. Yan, M. Bloom, S.C. Bae, E. Luijten, S. Granick, Linking synchronization to self-assembly using magnetic Janus colloids, Nature 491 (2012) 578.
[61] S. Li, H. Jiang, Z. Hou, Effects of hydrodynamic interactions on the crystallization of passive and active colloidal systems, Soft Matter 11 (28) (2015) 5712–5718.
[62] R.H. French, V.A. Parsegian, R. Podgornik, R.F. Rajter, A. Jagota, J. Luo, D. Asthagiri, M.K. Chaudhury, Y.-M. Chiang, S. Granick, S. Kalinin, M. Kardar, R. Kjellander, D.C. Langreth, J. Lewis, S. Lustig, D. Wesolowski, J.S. Wettlaufer, W.-Y. Ching, M. Finnis, F. Houlihan, O.A. von Lilienfeld, C.J. van Oss, T. Zemb, Long range interactions in nanoscale science, Rev. Mod. Phys. 82 (2) (2010) 1887–1944.
[63] D.W. Sinkovits, E. Luijten, Nanoparticle-controlled aggregation of colloidal tetrapods, Nano Lett. 12 (4) (2012) 1743–1748.
[64] N.M. Schneider, M.M. Norton, B.J. Mendel, J.M. Grogan, F.M. Ross, H.H. Bau, Electron–water interactions and implications for liquid cell electron microscopy, J. Phys. Chem. C 118 (38) (2014) 22373–22382.
[65] S.W. Chee, Z. Baraissov, N.D. Loh, P.T. Matsudaira, U. Mirsaidov, Desorption-mediated motion of nanoparticles at the liquid–solid interface, J. Phys. Chem. C 120 (36) (2016) 20462–20470.
[66] Q. Chen, H. Cho, K. Manthiram, M. Yoshida, X. Ye, A.P. Alivisatos, Interaction potentials of anisotropic nanocrystals from the trajectory sampling of particle motion using in situ liquid phase transmission electron microscopy, ACS Cent. Sci. 1 (1) (2015) 33–39.
[67] T.D. Nguyen, E. Jankowski, S.C. Glotzer, Self-assembly and reconfigurability of shape-shifting particles, ACS Nano 5 (11) (2011) 8892–8903.
[68] C.X. Du, G. van Anders, R.S. Newman, S.C. Glotzer, Shape-driven solid–solid transitions in colloids, Proc. Natl. Acad. Sci. USA 114 (20) (2017) E3892–E3899.
[69] F. Tu, D. Lee, Shape-changing and amphiphilicity-reversing Janus particles with pH-responsive surfactant properties, J. Am. Chem. Soc. 136 (28) (2014) 9999–10006.
[70] D. Klinger, C.X. Wang, L.A. Connal, D.J. Audus, S.G. Jang, S. Kraemer, K.L. Killops, G.H. Fredrickson, E.J. Kramer, C.J. Hawker, A facile synthesis of dynamic, shape-changing polymer particles, Angew. Chem., Int. Ed. 53 (27) (2014) 7018–7022.
[71] M. Youssef, T. Hueckel, G.-R. Yi, S. Sacanna, Shape-shifting colloids via stimulated dewetting, Nat. Commun. 7 (2016) 12216.
[72] E. Epstein, J. Yoon, A. Madhukar, K.J. Hsia, P.V. Braun, Colloidal particles that rapidly change shape via elastic instabilities, Small 11 (45) (2015) 6051–6057.
[73] J. Kim, X. Song, A. Kim, B. Luo, J.W. Smith, Z. Ou, Z. Wu, Q. Chen, Reconfigurable polymer shells on shape-anisotropic gold nanoparticle cores, Macromol. Rapid Commun. 39 (14) (2018) 1800101.
[74] D. Rus, M.T. Tolley, Design, fabrication and control of origami robots, Nat. Rev. Mater. 3 (6) (2018) 101–112.

[75] H. Fu, K. Nan, W. Bai, W. Huang, K. Bai, L. Lu, C. Zhou, Y. Liu, F. Liu, J. Wang, M. Han, Z. Yan, H. Luan, Y. Zhang, Y. Zhang, J. Zhao, X. Cheng, M. Li, J.W. Lee, Y. Liu, D. Fang, X. Li, Y. Huang, Y. Zhang, J.A. Rogers, Morphable 3D mesostructures and microelectronic devices by multistable buckling mechanics, Nat. Mater. 17 (3) (2018) 268–276.

[76] W. Huang, S. Koric, X. Yu, K.J. Hsia, X. Li, Precision structural engineering of self-rolled-up 3D Nanomembranes guided by transient quasi-static FEM modeling, Nano Lett. 14 (11) (2014) 6293–6297.

[77] X. Li, Strain induced semiconductor nanotubes: from formation process to device applications, J. Phys. D 41 (19) (2008) 193001.

[78] X. Li, Self-rolled-up microtube ring resonators: a review of geometrical and resonant properties, Adv. Opt. Photonics 3 (4) (2011) 366–387.

[79] F. Li, Z. Mi, Optically pumped rolled-up InGaAs/GaAs quantum dot microtube lasers, Opt. Exp. 17 (22) (2009) 19933–19939.

[80] Y. Mei, A.A. Solovev, S. Sanchez, O.G. Schmidt, Rolled-up nanotech on polymers: from basic perception to self-propelled catalytic microengines, Chem. Soc. Rev. 40 (5) (2011) 2109–2119.

[81] J. Aizenberg, P.V. Braun, P. Wiltzius, Patterned colloidal deposition controlled by electrostatic and capillary forces, Phys. Rev. Lett. 84 (13) (2000) 2997–3000.

[82] X. Yu, W. Huang, M. Li, T.M. Comberiate, S. Gong, J.E. Schutt-Aine, X. Li, Ultra-small, high-frequency, and substrate-immune microtube inductors transformed from 2D to 3D, Sci. Rep. 5 (2015) 9661.

[83] W. Huang, J. Zhou, P. Froeter, K. Walsh, S. Liu, J. Michaels, M. Li, S. Gong, X. Li, CMOS-compatible on-chip self-rolled-up inductors for RF/mm-wave applications, in: IEEE MTT-S International Microwave Symposium (IMS), 2017, pp. 1645–1648.

[84] W. Huang, J. Zhou, P.J. Froeter, K. Walsh, S. Liu, M.D. Kraman, M. Li, J.A. Michaels, D.J. Sievers, S. Gong, X. Li, Three-dimensional radio-frequency transformers based on a self-rolled-up membrane platform, Nat. Electron. 1 (5) (2018) 305–313.

[85] P. Froeter, Y. Huang, O.V. Cangellaris, W. Huang, E.W. Dent, M.U. Gillette, J.C. Williams, X. Li, Toward intelligent synthetic neural circuits: directing and accelerating neuron cell growth by self-rolled-up silicon nitride microtube array, ACS Nano 8 (11) (2014) 11108–11117.

[86] Z. Ou, X. Song, W. Huang, X. Jiang, S. Qu, Q. Wang, P.V. Braun, J.S. Moore, X. Li, Q. Chen, Colloidal metal–organic framework hexapods prepared from postsynthesis etching with enhanced catalytic activity and rollable packing, ACS Appl. Mater. Interfaces 10 (48) (2018) 40990–40995.

[87] Z. Tian, B. Xu, B. Hsu, L. Stan, Z. Yang, Y. Mei, Reconfigurable vanadium dioxide nanomembranes and microtubes with controllable phase transition temperatures, Nano Lett. 18 (5) (2018) 3017–3023.